DOI: https://doi.org/10.14311/TPFM.2025.012

3D UNSTEADY MOTION AND DEFORMATION OF A GAS BUBBLE IN VIBRATING LIQUID UNDER ZERO GRAVITY

C. Galusinki [1], T.P. Lyubimova [2,3], S. Meradji [1]

[1] **Laboratoire IMATH - EA 2134, Université de Toulon, 83130 La Garde, France**

[2] **Department of Theoretical Physics, Perm State University, 614990 Perm, Russia**

[3] **Institute of Continuous Media Mechanics, Ural Branch of the Russian Academy of Science, 614013 Perm, Russia**

Abstract

Numerical investigation of a bubble immersed in a liquid of different density inside a container subjected to translational oscillations under weightlessness reveals the following scenario: the bubble, initially centered, moves toward the container wall due to a non-viscous attraction mechanism. This motion is accompanied by small-amplitude oscillations at the forcing frequency and long-period eigen-oscillations induced by the initial acceleration. Concurrently, the bubble shape deforms, averaging over the forcing period, with flattening along the vibration axis and, under certain conditions, exhibiting parametric oscillations. A notable deceleration occurs as the bubble approaches the wall, stopping at a finite distance from the wall, without making contact.

Keywords: drops (bubbles), interfacial flows, instability, level set method.

1 Introduction

The present work is devoted to the numerical investigation in 3D of the influence of harmonic translational vibrations on two-phase fluid system (liquid in coexistence with its vapor) when gravity effects are absent. In addition to the obvious interest of investigating fluid behavior under new conditions, the study was also motivated by the need to manage fluids in spatial conditions. In such conditions, gravity is often absent and vibration often present, making the vapor and liquid phase localization uncertain. It can become important to know whether the vapor phase is present as a bubble in the center of the container or compressed against a wall. Vibrations can help, as outlined in this work. Some experiments have already been performed under low gravity conditions - near the critical point - onboard a sounding rocket in CO_2, in the MIR station in SF_6, and in H_2 under magnetic compensation of earth gravity [1]. Average effects such as average shape deformation and average displacement of the bubble were observed. A wall attraction mechanism having non-viscous origin is thus expected. The case of an inclusion near a planar vibrating wall without the confinement effect has been previously investigated neglecting the viscosity. It was shown that the wall attracts the inclusion, with a force that increases when the distance between the wall and inclusion decreases [2, 3, 4]. When a bubble surrounded by a liquid of different density is subject to vibrations, it may respond in different ways. Since the bubble is an oscillatory (elastic) system, one expects the excitation of eigen and forced oscillations. Some of these phenomena were observed with drops under acoustic fields [5]. The oscillations of a bubble (drop) surrounded by a fluid of different density in a container subjected to the translational vibrations with linear polarization were also studied. It was found that specific parametric resonance (synchronism condition) takes place at the forcing frequency equal to the sum of two neighboring eigen-oscillations modes of the drop (bubble) [6]. Additionally, time-averaged behavior of the bubble (drop) was studied. The effects of average flattening of the drop in the direction of vibration wall were discovered [7, 8]. Finally, the dynamics of two-phase system vapor bubble in equilibrium with its liquid phase under translational vibrations, in the absence of gravity, was recently investigated theoretically and numerically in an attempt to reproduce the experiments related to SF_6 and H_2 fluids [9]. A 2D geometrical approximation was used (two coaxial cylinders) in [9]. The aim of this preliminary work is to extend the performed analysis in 3D (spherical bubble in a cylindrical container). Only H_2 fluid will be considered here.

2 Mathematical model and numerical approach

2.1 General

A cylindrical cell filled with an isothermal liquid-vapor two-phase system, without phase change, under weightlessness conditions (no gravity) is considered here. The cell undergoes sinusoidal translational oscillations in the plane perpendicular to the cylinder axis as depicted in Fig. 1.

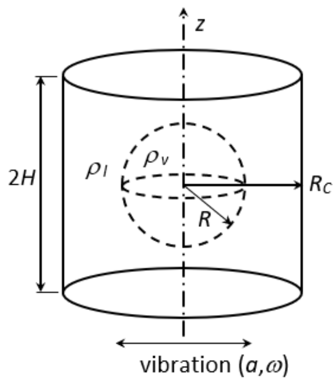

Figure 1: Geometry of the container with the vapor bubble (interrupted lines).

The bubble motion and the deformation of its liquid-vapor interface is investigated. In the numerical simulation, it is assumed that the vapor inclusion is initially at the center of symmetry of the container. The inclusion size is comparable to the container size. In absence of gravity and vibrations, the inclusion is of spherical shape. The temperature of the system is taken not too close to the critical temperature, such that both phases can be considered as incompressible and the density values of the phases are assumed to be close. For the two-phase configuration assumed in the present study, one thus could expect that the bubble, initially located at the symmetry center of the system, would be attracted preferably by the closest wall when vibration starts. For the vibrational velocity amplitudes exceeding some threshold, one can also expect parametric resonance oscillations of the liquid-vapor interface.

2.2 Basic equations

When considering two incompressible Newtonian fluids, the model reads

$$\rho\left(\frac{\partial \mathbf{u}}{\partial t}+\mathbf{u}\cdot\nabla\mathbf{u}\right)-\nabla\cdot(2\mu D\mathbf{u})+\nabla p=\mathbf{F}\quad\forall(t,\mathbf{x})\in\mathbb{R}^+\times\Omega, \tag{1}$$

with the incompressibility condition

$$\nabla\cdot\mathbf{u}=0\quad\forall(t,\mathbf{x})\in\mathbb{R}^+\times\Omega, \tag{2}$$

where the field $\mathbf{u}=(u,v,w)$ is the velocity, p the pressure, ρ the density, μ the viscosity, $\mathbf{F}$ any body force detailed hereafter and $D\mathbf{u}=(\nabla\mathbf{u}+\nabla^T\mathbf{u})/2$. The domain Ω is defined thanks to a signed distance function φ, nonnegative inside Ω. The model will be perturbed to be defined on $\Omega_\varepsilon\subset\Omega$ to anticipate an immersed boundary method due to a mesh which does not fit to the geometry. A modified boundary condition is imposed on the boundary of Ω_ε (the one fitted with the mesh) using the information of the distance function to the real domain Ω. The Level Set approach is also used to identify fluid 1 and fluid 2 across a signed distance function ψ negative in fluid 1 and positive in fluid 2. The two fluids are transported by the flow,

$$\frac{\partial\psi}{\partial t}+\mathbf{u}\cdot\nabla\psi=0\quad\forall(t,\mathbf{x})\in\mathbb{R}^+\times\Omega_\varepsilon. \tag{3}$$

The force $\mathbf{F}$ includes vibration and surface tension forces,

$$\mathbf{F}_\sigma = \rho(\psi) a\omega^2 \sin(\omega t + \phi)\mathbf{k} + \sigma\kappa\delta(\psi)\mathbf{n}, \tag{4}$$

where δ denotes the Dirac measure supported by the interface $\{\psi = 0\}$, $\kappa = \nabla \cdot \frac{\nabla\psi}{|\nabla\psi|}$ the mean curvature of the interface, $\omega = 2\pi f$ the angular frequency, f the frequency, a the amplitude of vibrations, ϕ the phase shift and $\mathbf{k}$ the vector unit of the vibration direction. The unified bifluid model has been introduced in [10] and can be written, in the frame of the vibrating container, under linear vibrations assumption ($a \ll R_c$), as

$$\begin{aligned}
&\rho(\psi)\left(\frac{\partial \mathbf{u}}{\partial t} + \mathbf{u}\cdot\nabla\mathbf{u}\right) - \nabla\cdot(2\mu(\psi)D\mathbf{u}) + \nabla p = \rho(\psi)a\omega^2\sin(\omega t+\phi)\mathbf{k} + \sigma\kappa\nabla H(\psi), \text{ in } \mathbb{R}^+\times\Omega_\varepsilon \\
&\nabla\cdot\mathbf{u} = 0 \quad \text{in } \mathbb{R}^+\times\Omega_\varepsilon \\
&-\varphi\nabla\mathbf{u}\cdot\nabla\varphi + \mathbf{u} = 0, \text{ in } \mathbb{R}^+\times\partial\Omega_\varepsilon,
\end{aligned} \tag{5}$$

The Heavyside function H is regularized when considering the discrete model.

Before solving the non-conservative formulation (5), we first modify the surface tension term. By applying a change of function in the pressure variable, the Dirac delta function is eliminated from the surface tension term, allowing division by density to be performed.

$$\kappa\nabla H(\psi) = \nabla(\kappa H(\psi)) - H(\psi)\nabla\kappa.$$

We can then replace the first equation of (5) with

$$\frac{\partial \mathbf{u}}{\partial t} + \mathbf{u}\cdot\nabla\mathbf{u} - \frac{1}{\rho(\psi)}\nabla\cdot(2\mu(\psi)D\mathbf{u}) + \frac{1}{\rho(\psi)}\nabla(p - \sigma\kappa H(\psi)) = a\omega^2\sin(\omega t+\phi)\mathbf{k} - \frac{\sigma}{\rho(\psi)}H(\psi)\nabla\kappa, \tag{6}$$

2.3 Numerical method

Equation (6) is suitable for a velocity prediction assuming that the pressure is known. A classical algorithm based on prediction-correction (projection method [11]) can follow. In the prediction step, a classical MAC scheme on a staggered grid [12] meshing Ω_ε uses the modified boundary condition on the boundary

$$-\varphi\nabla\mathbf{u}\cdot\nabla\varphi + \mathbf{u} = 0, \text{ in } \mathbb{R}^+\times\partial\Omega_\varepsilon,$$

which corresponds to an immersed boundary method at order 2 with a decenterd discretization of $\nabla\mathbf{u}$ on the boundary inside the domain. In the correction step, an anisotropic Poisson problem has to be solved on Ω_ε, the pressure correction $\tilde{p}$ solves,

$$\nabla\cdot(\frac{1}{\rho(\psi)}\nabla\tilde{p}) = \nabla\cdot\tilde{\mathbf{u}}, \tag{7}$$

with Neumann boundary condition, where $\tilde{\mathbf{u}}$ is the predicted velocity of the projection method. Furthermore, the term $\frac{1}{\rho(\psi)}\nabla\tilde{p}$ affects the velocity in (6) and the space discretizations of (6) and (7) have to be compatible. The mesh of Ω_ε corresponds to the pressure mesh, and normal velocities are on the faces of the pressure cell. In order to solve (7) with a finite-volume scheme ensuring flux continuity, the density $\rho(\psi)$ has to be defined on a control volume surrounding each normal velocity face. Finally, each component of $\frac{1}{\rho(\psi)}\nabla\tilde{p}$ is accurately defined on each face of the pressure mesh, as the velocity components. The linear system involved by the Poisson equation is solved with a fast multigrid solver [13] or BiCGstab algorithm to deal with large ratio of fluid densities. Details and validations of this numerical solver are given in [14].

3 Parameters study

This section concerns a vapor bubble under vibrations as used in experiments with H_2. The parameters values are chosen to satisfy both the experimental and simulation constraints [9].

3.1 Physical properties

The experiments with hydrogen were performed at the typical cryogenic temperatures of 500 mK and 200 mK below the critical temperature $T_c = 33.19\,\mathrm{K}$. The data are summarized in table 1.

Density	Temperature behavior	
	$T - T_c = -500$ mK	$\rho_l = 44.39$, $\rho_v = 18.46$ (kg/m^3)
	$T - T_c = -200$ mK	$\rho_l = 41.05$, $\rho_v = 21.80$ (kg/m^3)
Dynamic Viscosity	Temperature behavior	
	$T - T_c = -500$ mK	$\mu_l = 4.75 \times 10^{-6}$, $\mu_v = 1.98 \times 10^{-6}$ (Pa · s)
	$T - T_c = -200$ mK	$\mu_l = 4.39 \times 10^{-6}$, $\mu_v = 2.33 \times 10^{-6}$ (Pa · s)
L-V interfacial tension	Temperature behavior	
	$T - T_c = -500$ mK	$\sigma(T) = 2.890 \times 10^{-5}$ (N/m)
	$T - T_c = -200$ mK	$\sigma(T) = 0.912 \times 10^{-5}$ (N/m)

Table 1: Physical properties of H_2 [15]. The subscript l denotes liquid and v, vapor.

3.2 Numerical simulation scenarios

The geometrical and vibrational conditions used to simulate the experiments are given in table 2. As one can see, the restrictions $a \ll R_c$ – $\sqrt{2\mu/(\rho\omega)} \ll R_c$ are satisfied here. Vibrations could thus be considered as being of (i) small-amplitude and (ii) high-frequency (but not acoustic) and the results can be successfully described by the theory developed in the small-amplitude and high-frequency low viscosity approach [7, 8].

Container	Radius	$R_c = 1.5$ mm
	Half-height	$H = 1.5$ mm
	Aspect ratio	$H/R_c = 1$
Inclusion	radius, R	0.75 mm
	N.D. radius, R/R_c	1/2
	Surfacic occupation, $(R/R_c)^2$	0.250
	Volumic occupation, $(2/3)(R_c/H)(R/R_c)^3$	≈ 0.085
Vibration	amplitude	$a = [0.05 - 0.40]$ mm
	frequency	$f = [20 - 45]$ Hz

Table 2: Geometrical and vibrational conditions for the simulation of H_2 experiments [9].

A few scenarios in terms of vibration frequency and amplitude have been chosen for a single small size bubble ($R/R_c = 0.5$), taking into account the conditions of the linear stability analysis and the synchronism condition frequency calculations [6]. The forcing vibration frequency was thus chosen with respect to the resonance condition for the single bubble size value scenario $R/R_c = 0.5$ and at two distances from the critical temperature, $(T - T_c) = -500$ mK and -200 mK (Table 1). The condition for the excitation of the parametric resonance should be the same for spherical and cylindrical inclusions. Most of the scenarios therefore consist in varying the vibration amplitude around the threshold value (in amplitude) beyond which parametric oscillations are expected. As already noted, for reasons of drop stability, the vibration amplitude had to be limited ($a = [0.05 - 0.40]$ mm). Another scenario consists in varying the vibration frequency for a given value of the vibration amplitude. Substituting the values of the eigen frequencies calculated in [6] for the two-phase system H_2 at $(T - T_c) = -500$ mK, one obtains for $R/R_c = 1/2$: $f_2 \approx 12.3$ Hz, $f_3 \approx 25.5$ Hz, $f_{res,2-3} \approx 37.8$ Hz. At $(T - T_c) = -200$ mK, one obtains for $R/R_c = 1/2$: $f_2 \approx 6.93$ Hz, $f_3 \approx 14.3$ Hz, $f_{res,2-3} \approx 21.2$ Hz. Numerical simulations are conducted with vibrating container frequencies closely matching the theoretical predictions from the synchronism condition: $f = 38.5$ Hz at $(T - T_c) = -500$ mK and $f = 20$ Hz at $(T - T_c) = -200$ mK.

4 Numerical results

Numerical simulations were conducted using the vibrational parameters, physical properties, and geometrical conditions listed in Tables 1 and 2. In all cases, amplitude and frequency were varied at a constant bubble volume fraction ($R/R_c = 1/2$), with an initial phase shift $\phi = \pi/2$. Figures 2 and 3 depict the time evolution of the bubble's center of mass for selected vibration amplitudes at fixed temperature (at a specified distance from the critical point) and frequencies (38.5 Hz and 20 Hz, respectively). Figure 4 shows the effect of varying vibration frequency at a fixed moderate amplitude ($a = 0.250$ mm) and temperature $(T - T_c) = -500$ mK, as in Figure 2.

As shown, all curves display small-amplitude oscillations at the forcing frequency, with the bubble exhibiting distinct long-term behaviors. Initially positioned at the container center, the bubble is immediately propelled in the direction of the initial impulse ($x < 0$) and then shifts on average towards the $x > 0$ side, as explained by a mechanical model [9]. Mainly, two situations are observed: (i) at low to moderate vibration velocity values, $a\omega$, the bubble performs moderate-amplitude damped oscillations with a large period around a quasi-equilibrium position at a finite distance from the wall, tending to stabilize closer to the center as the amplitude decreases; and (ii) at high $a\omega$ values, the initial position becomes unstable, and the bubble moves towards and stabilizes near the closest wall in quasi-contact, consistent with theoretical predictions [2].

An interesting finding is the bubble's deceleration as it approaches the wall, stopping without making contact, as illustrated in Figure 7. In this final state, the bubble remains nearly stationary, performing small oscillations around its mean position. The quasi-equilibrium distance from the wall decreases with increasing vibration frequency (due to the reduced Stokes boundary layer thickness) and/or amplitude. Figure 2 confirms that the forced oscillation amplitude increases with vibration amplitude for a fixed pulsation $\omega = 2\pi f$, in agreement with theoretical expectations [9]. Conversely, Figure 4 shows that the forced oscillation amplitude decreases with increasing pulsation at a fixed vibration amplitude.

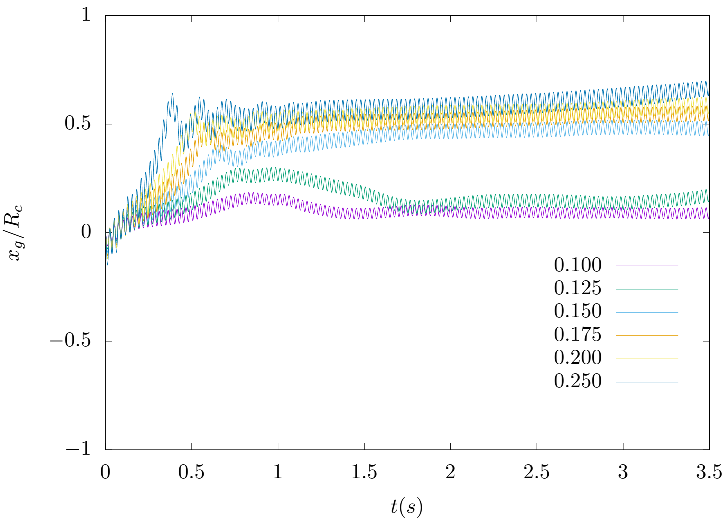

Figure 2: Time-evolution of reduced bubble center of mass coordinates (x_g/R_c), for $f = 38.5$ Hz and different values of amplitude a (mm). Case $R/R_c = 1/2$, $(T - T_c) = -500$ mK and $\phi = \pi/2$.

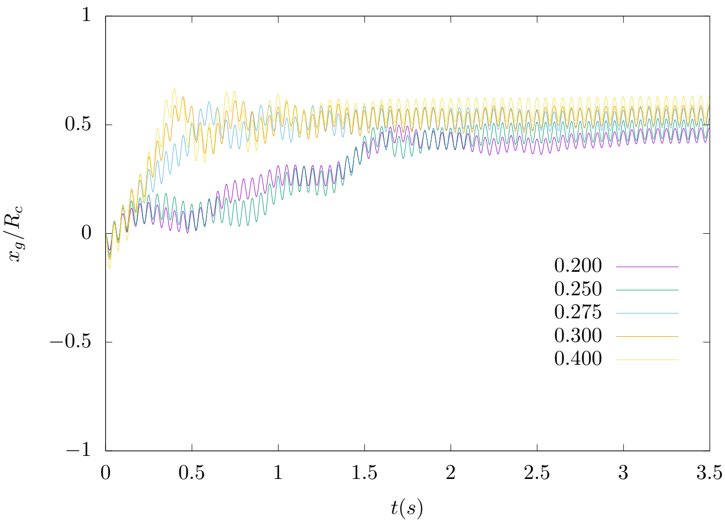

Figure 3: Time-evolution of reduced bubble center of mass coordinate (x_g/R_c), for $f = 20$ Hz and different values of amplitude a (mm). Case $R/R_c = 1/2$, $(T - T_c) = -200$ mK and $\phi = \pi/2$.

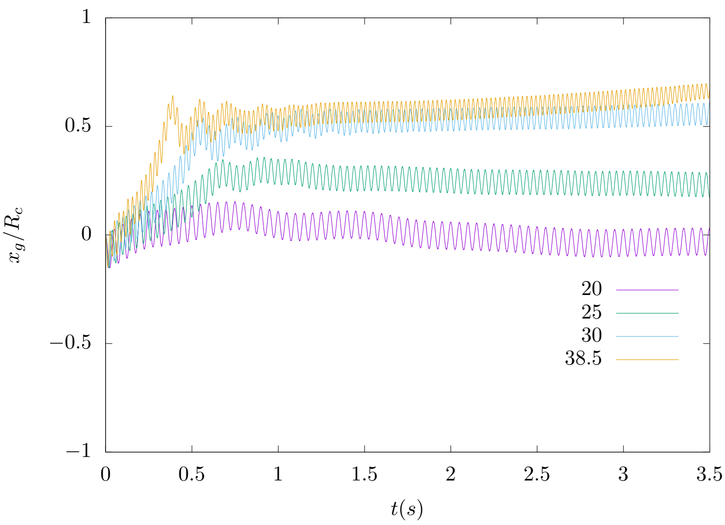

Figure 4: Time-evolution of reduced bubble center of mass coordinate (x_g/R_c), for $a = 0.250$ mm and different values of frequency f (Hz). Case $R/R_c = 1/2$, $(T - T_c) = -500$ mK and $\phi = \pi/2$.

Figures 5 and 6 show the time evolution of the bubble's center of mass in three spatial directions for different vibrational conditions and distances from T_c. The left panels correspond to $(T - T_c) = -500$ mK, while the right panels represent -200 mK. Vibrational conditions are chosen such that the velocity amplitude, $a\omega$, is nearly identical in both cases. The 3D bubble dynamics, captured through the motion of its center of mass, differs significantly when the frequency increases from 20 Hz to 38.5 Hz. At higher frequencies, the bubble tends to reach the edge faster in a direction other than the vibration axis (primarily along Oz, as seen in the left panels), despite its low volume fraction (Table 2). Consequently, oscillation amplitudes over longer periods are smaller at higher frequencies (right panels). Over time, bubbles stabilize, reaching equilibrium either at a finite distance from the wall or near it.

Figure 7 provides a perspective view of the instantaneous bubble shape, initially spherical and centered in the container, for a vibration amplitude of 0.400 mm at 200 mK from T_c. The bubble flattens along the vibration axis (e.g., at $t = 0.168$ s) and undergoes parametric oscillations, alternating between two- and three-lobed shapes (e.g., at $t = 0.130$ s and $t = 0.476$ s). In the right panel of Figure 6, the associated time evolution of the bubble's center of mass in three spatial directions further illustrates its global dynamics. The theoretically predicted average deformation of the bubble over the forcing period is also observed numerically.

A bubble fragmentation scenario occurs when the vibration amplitude exceeds 0.250 mm at frequency $f = 38.5$ Hz and 500 mK below T_c. At lower amplitudes ($a = 0.150$ mm and 0.175 mm), with $f = 20$ Hz and 200 mK from T_c, surface waves also appear on the bubble. However, these observations require further investigation and are not presented here.

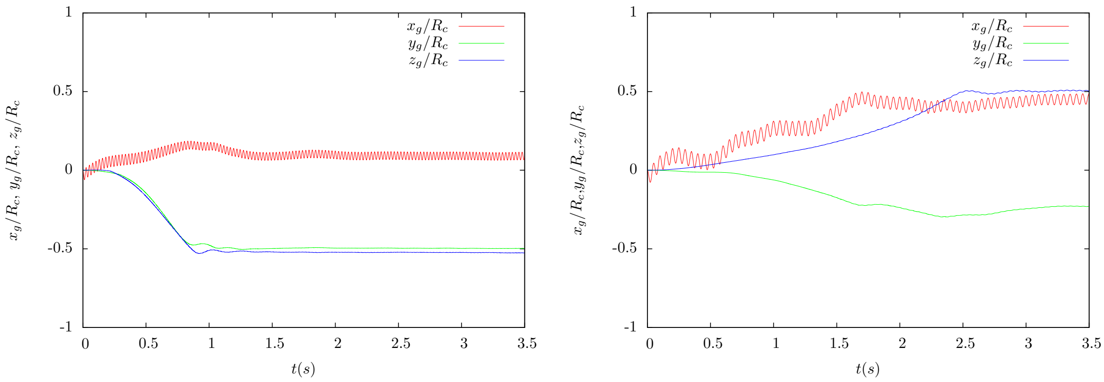

Figure 5: Time-evolution of reduced bubble center of mass coordinates (x_g/R_c, y_g/R_c, z_g/R_c):
- Case $R/R_c = 1/2$, $\phi = \pi/2$, $(T - T_c) = -500$ mK, $a = 0.100$ mm and $f = 38.5$ Hz (left)
- Case $R/R_c = 1/2$, $\phi = \pi/2$, $(T - T_c) = -200$ mK, $a = 0.200$ mm and $f = 20$ Hz (right)

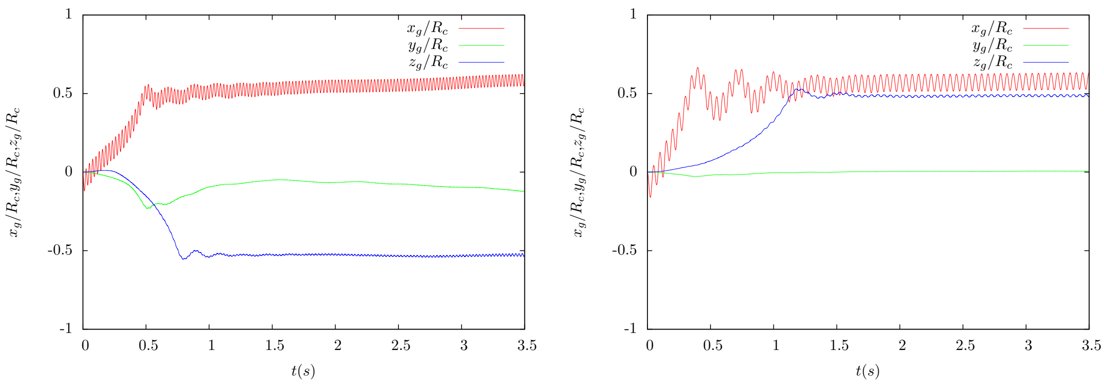

Figure 6: Time-evolution of reduced bubble center of mass coordinates (x_g/R_c, y_g/R_c, z_g/R_c):
- Case $R/R_c = 1/2$, $\phi = \pi/2$, $(T - T_c) = -500$ mK, $a = 0.200$ mm and $f = 38.5$ Hz (left)
- Case $R/R_c = 1/2$, $\phi = \pi/2$, $(T - T_c) = -200$ mK, $a = 0.400$ mm and $f = 20$ Hz (right)

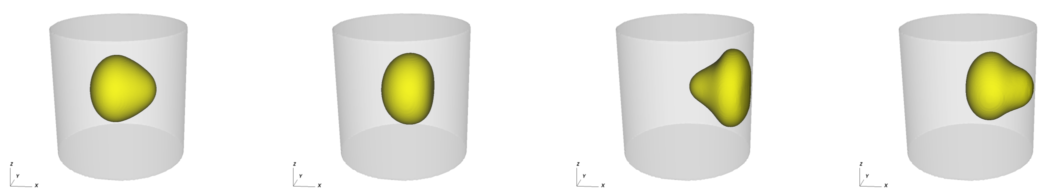

Figure 7: Perspective view of the vibrating container with the bubble at different instants.
Case $R/R_c = 1/2$, $(T - T_c) = -200$ mK, $a = 0.400$ mm, $f = 20$ Hz and $\phi = \pi/2$:
$t = 0.130$ s ; $t = 0.168$ s ; $t = 0.450$ s ; $t = 0.476$ s (from left to right)

5 Conclusion

The dynamics of a vapor bubble in equilibrium with its liquid phase, subjected to harmonic translational vibrations under weightlessness, is analyzed numerically in 3D. The system is confined in a cylindrical container vibrating perpendicular to its axis. Initially, the bubble is positioned at the container's center. The study focuses on vibrational conditions relevant to experiments on a two-phase para-Hydrogen (H_2) system near its critical point, conducted under magnetic compensation of gravity. Both liquid and vapor phases are treated as viscous and incompressible. Under small-amplitude, high-frequency vibrations, numerical results reveal forced translational oscillations at the driving frequency. Besides the flattening of the bubble along the vibration axis, a time-averaged shape deformation is observed. The bubble's initial position at the center is an unstable quasi-equilibrium. When vibrations are applied, the bubble drifts towards the wall. At high values of $a\omega$, the bubble reaches the wall and, after brief large-scale oscillations, performs only forced oscillations near the wall. The quasi-equilibrium distance from the wall grows as vibration frequency decreases. For moderate $a\omega$, the bubble stabilizes at a finite distance from the wall, where it undergoes damped, large-scale oscillations superimposed with forced oscillations. The amplitude and period of these large-scale oscillations diminish as $a\omega$ decreases, with faster damping at higher $a\omega$. This work provides insights into the behavior of two-phase systems under vibrations and lays the groundwork for future studies in microgravity fluid mechanics.

Acknowledgment

Centre de Calcul Intensif d'Aix-Marseille is acknowledged for granting access to its high performance computing resources.

References

[1] Wunenburger, R., Chatain, D., Garrabos, Y., Beysens, D.: Magnetic compensation of gravity forces in hydrogen near its critical point. *Phys. Rev. E* **62**, (2000), 469-476.

[2] Lyubimov, D., Lyubimova, T., Cherepanov, A.: On a motion of solid body in a vibrating fluid. *Convective Flows. Collection of Perm State University* , (1987), 61-70.

[3] Lugovtsov, B.A., Sennitskiy, V.L.: Motion of body in vibrating fluid. *USSR Rept Eng Equipment. Transl. into English from Doklady Akademii Nauk SSSR (Moscow, USSR)* **289**, (1987), 314-317.

[4] Lyubimov, D., Cherepanov, A., Lyubimova, T.: The motion of solid body in a liquid under the influence of a vibrational field. *In Reviewed Proc. of the First Int. Symp. On Hydromechanics and Heat/Mass Transfer in Microgravity, Gordon and Breach* , (1992), 246-251.

[5] Marston, P.L.: Shape oscillation and static deformation of drops and bubbles driven by modulated radiation stress: theory. *J. Acoust. Soc. Amer.* **67**, (1980), 15-26.

[6] Lyubimov, D.V., Lyubimova, T.P., Cherepanov, A.A.: Resonance oscillations of a drop (bubble) in a vibrating fluid. *J. Fluid Mech.* **909**, (2021), A18/1-A18/19.

[7] Lyubimov, D.V., Cherepanov, A.A., Lyubimova, T.P.: Deformation of gas or drop inclusion in high frequency vibrational field. *Microgravity Quarterly* **6**, (1996), 69-73.

[8] Lyubimov, D.V., Cherepanov, A.A., Lyubimova, T.P., Roux, B.: Dynamics of Fluid Interfaces in Vibrational Fields. *Moscow, PhysMathLit*, (2003).

[9] Lyubimov, D.V., Lyubimova, T.P., Meradji, S., Roux, B.: Vibration-induced wall–bubble interactions under zero-gravity conditions. *Journal of Fluid Mechanics* **992**, (2024), A7.

[10] Sussman, M., Smereka, P., Osher, S.: A level set approach for computing solutions to incompressible two-phase flow. *J. Comput. Phys*, vol. 114, (1994), pp. 146–159.

[11] Guermond, J.L., Shen, J.: An overview of projection methods for incompressible flows. *Comput. Methods Appl. Mech. Engrg*, vol. 41, (2006), pp. 112–134.

[12] Harlow, F.H., Welch, J.E.: Numerical calculation of time-dependent viscous incompressible flow of fluid with free surface. *Physics of Fluids*, vol. 8(12), (1965), pp. 2182–2189.

[13] Notay, Y.: An aggregation-based algebraic multigrid method. *Electronic Transactions on Numerical Analysis*, vol. 37, (2010), pp. 123–146.

[14] Galusinski, C.: Problematic of Incompressible Bifluid Navier-Stokes Equations Approached on Non Body Fitted Meshes *Topical Problems of Fluid Mechanics*, (2016), pp. 51–58.

[15] Jouers, C.: Hydrogen properties for fusion energy. *Publ. Univ. of California Press*, (1986).